Journal of Power Sources 222 (2013) 477–482

Contents lists available at SciVerse ScienceDirect

Journal of Power Sources

journal homepage: www.elsevier.com/locate/jpowsour

Effects of ionomer content on Pt catalyst/ordered mesoporous carbon support in polymer electrolyte membrane fuel cells

Chi-Yeong Ahn [a], Jae-Yeong Cheon [b], Sang-Hoon Joo [b], Junbom Kim [a,*]

[a] School of Chemical Engineering & Bioengineering, University of Ulsan, Daehak-ro 93, Nam-gu, Ulsan 680-749, Republic of Korea
[b] School of Nano-Bioscience and Chemical Engineering and KIER-UNIST Advanced Center for Energy, Ulsan National Institute of Science and Technology (UNIST), UNIST-gil 50, Ulsan 689-798, Republic of Korea

HIGHLIGHTS

- Pt/OMC with high loading was synthesized for polymer electrolyte membrane fuel cells (PEMFCs).
- Electrodes with different ionomer loadings (in the range of 5–30 wt. %) with Pt/OMCs were applied in cathode.
- Pt particles placed on or between two or more carbon nanorods can share and utilize electrolytes.
- Excessive ionomer can trap H_2O generated by electrochemical reactions and cause mass transfer problems.
- 10 wt. % Ionomer with prepared Pt/OMCs is determined to be the optimum amount.

ARTICLE INFO

Article history:
Received 22 June 2012
Received in revised form
3 September 2012
Accepted 5 September 2012
Available online 10 September 2012

Keywords:
Polymer electrolyte membrane fuel cell
Ordered mesoporous carbon
Platinum
Catalyst
Nafion

ABSTRACT

In this paper, the optimum Nafion ionomer content in platinum (Pt) dispersed on ordered mesoporous carbon (OMC) catalyst is investigated. The ionomer content can affect catalytic activity, ionic conductivity and mass transfer characteristics. A nano-replication method using ordered mesoporous silicas (OMS) is applied to prepare OMCs, and Pt/OMC with high loading are synthesized by the incipient wetness method for polymer electrolyte membrane fuel cells (PEMFCs). Catalyst characteristics have been analyzed using TGA, XRD, TEM and BET. Cathode electrodes have different ionomer loadings (in the range of 5–30 wt. %) with Pt/OMCs. Commercial Pt/C catalyst is used in anode. All membrane electrode assemblies (MEAs) fabricated by the decal transfer method show about 0.4 mg cm^{-2} Pt loading. The PEMFC performances have been measured by electrochemical methods such as polarization curves, electrochemical impedance spectroscopy (EIS), and cyclic voltammetry (CV). The performances is different at low and high current density regions, and the optimum content of ionomer is 10 wt. % in the catalyst, due to unique structure of OMCs.

1. Introduction

A fuel cell is a device that converts chemical energy to electric energy directly from a chemical reaction of hydrogen and oxygen. In particular, polymer electrolyte membrane fuel cells (PEMFCs) are widely developed as power sources for vehicles and as small, localized power plants in other applications due to their low operation temperature [1]. Many studies of noble metals, alloys and supports have been conducted to improve the performance of fuel cells for use as catalysts in PEMFCs [2–10].

Among the various areas of catalyst research, the supports are one of the most important areas for improving performance. Support candidates for fuel cells should have good electrical conductivity, interaction between catalyst and support, water handling capability, corrosion resistance, large surface area, mesoporous structure, and easy catalyst recovery. A good interaction between the catalyst and support improves catalyst efficiency and decreases resistances in fuel cells [11].

Oil-furnace type carbon blacks (CBs), such as Vulcan XC-72R (Cabot Corp, 250 $m^2\ g^{-1}$), Black Pearl 2000 (BP2000, Cabot Corp., 1500 $m^2\ g^{-1}$), Ketjen Black (KB EC600JD and KB EC600J, Ketjen International, 1270 $m^2\ g^{-1}$ and 800 $m^2\ g^{-1}$, respectively) and acetylene black type CBs such as Shawinigan (Chevron, 80 $m^2\ g^{-1}$), and Denka Black (DB, Denka, 65 $m^2\ g^{-1}$) are widely used for supports to ensure a large electrochemical active surface area [11,12]. In addition, carbon based nanostructures like carbon nanotubes (CNTs), carbon nanofibers (CNFs), mesoporous carbon, nanodiamonds and grapheme have been described as catalyst

* Corresponding author. Tel.: +82 52 259 2833; fax: +82 52 259 1689.
E-mail address: jbkim@mail.ulsan.ac.kr (J. Kim).

0378-7753/$ – see front matter © 2012 Elsevier B.V. All rights reserved.
http://dx.doi.org/10.1016/j.jpowsour.2012.09.012

supports [9,10,13–15]. These carbon allotropes have essential properties required to support in fuel cells such as high specific surface area, high electrical conductivity and good stability in acid and alkaline media.

Ordered mesoporous carbons (OMCs) consisting of periodic arrays of carbon nanorods with uniform mesopores are strong candidates for catalyst support in PEMFCs due to their high specific surface areas, uniform pore diameters, and high thermal, chemical and mechanical stabilities [13,16]. OMCs can be utilized as catalyst supports because they can be synthesized from many kinds of carbon sources such as sucrose, naphthalene, anthracene, pyrene, benzene and phenanthrene. Different OMCs show different physical and chemical characteristics [17,18]. Different silica sources are also used to prepare Pt/OMCs, and show better performance than commercial Pt/C [19]. Many studies of Pt/OMCs have focused on improving the performance of PEMFCs [20–23].

The addition of Nafion in the electrode improves the performance of PEMFCs by increasing the three-phase boundary, so optimum Nafion content in the catalyst layer is important to achieve good performance. An insufficient amount of Nafion in the catalyst layer results in poor contact of the electrolyte with the catalyst and reduces the triple-phase boundary. Excessive quantities of Nafion also cause a decrease in performance by blocking the active catalyst sites and reducing the gas permeability [24,25]. Optimum ionomer content depends on the type of support (e.g., carbon black and CNTs), Pt loading (e.g., 0.4 mg cm^{-2} and 1.0 mg cm^{-2}), weight percent Pt (e.g., 20 wt. % and 40 wt. % Pt/support), catalysts (e.g., Pt and alloy) and operating conditions (e.g., different relative humidity) that are used [26–38]. Jeon et al. [38] showed that 30 wt. % ionomer in the electrode resulted in the best performance at 0.6 V and that 20 wt. % ionomer showed the best performance at 0.4 V due to the combined effect of platinum utilization and oxygen gas transport with highly humidified atmospheric air.

In this study, we investigated the optimum content of Nafion ionomer into Pt dispersed on OMCs having an intrinsic structure. Pt/OMC (50 wt. %) was synthesized, and its characteristics were analyzed by a thermo gravimetric analyzer (TGA), X-ray diffraction (XRD), a transmission electron microscope (TEM) and the Brunauer, Emmet, and Teller (BET). Pt/OMCs and commercial Pt/C catalyst were applied in the cathode and anode, respectively. All MEAs were fabricated by the decal transfer method. The performances of MEAs were measured by polarization curves, EIS, and CV.

2. Experimental

2.1. Synthesis of OMCs

OMS having a hexagonal structure and large pores was synthesized following a previously reported method [16,18] using Pluronic P123 triblock copolymer (Aldrich). A sodium silicate solution of Na/Si = 2.5 (10 wt.% SiO_2) was prepared as a silica source using colloidal silica Ludox HS-40 (Aldrich, 40 wt.% SiO_2), sodium hydroxide, and deionized water. After mixing P123 and the sodium silicate solution in deionized water, the mixture was placed in a flask with a water jacket and stirred at ambient temperature. To polymerize the silicate species, acetic acid (JT Baker) solution in deionized water was added. The mixture was stirred at 318 K for 20 h and placed in an oven at 373 K for 24 h. The silica precipitate was filtered, washed with deionized water, and dried in a vacuum desiccator. Finally, the resulting material was calcined with air at 823 K for 3 h.

To replicate OMC, sucrose precursors were used with the synthesized OMS template. The synthesis of OMC, CMK-3, was described previously [16]. A carbon precursor solution was obtained by dissolving a 1.25 g of sucrose, 0.14 g of sulfuric acid and 5 g of deionized water. Applying an incipient wetness method, the precursor solution was impregnated into 1 g of the OMS template and the mixture was dried first at 373 K and subsequently at 433 K. To infiltrate almost all of the internal pores of the OMS template with CMK-3 carbon sources, the impregnation-drying step was repeated twice. Heating at 1373 K under nitrogen flow for 2 h was carried out for carbonization of CMK-3. Finally, 10% HF in a deionized water–ethanol solution was applied to dissolve the silica templates at room temperature.

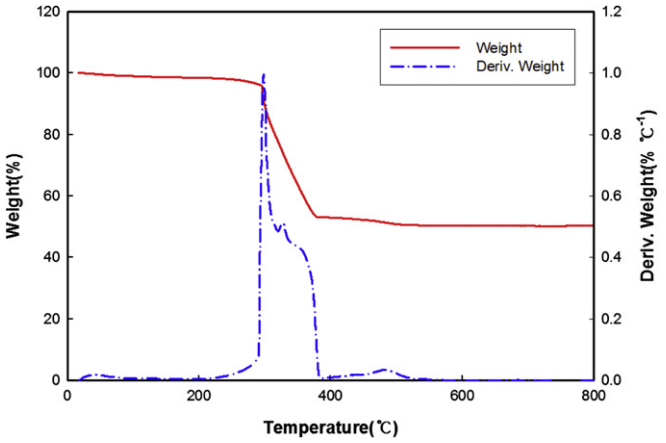

Fig. 1. TGA results of prepared Pt/OMCs.

2.2. Preparation of Pt/OMCs catalyst

OMC (0.5 g) was mixed with $H_2PtCl_6 \cdot xH_2O$ (Umicore) containing 1.5 ml acetone as a Pt precursor by the incipient wetness method. The amount of Pt precursor in the solution was controlled to obtain a Pt loading of 50 wt. % Pt/OMCs. After being dried in a 333 K oven for 24 h, the OMC with Pt oxide was reduced in flowing H_2 to 473 K and kept for 2 h at the same temperature. The adsorbed hydrogen was removed by heating to 623 K and was kept for 3 h under an argon flow.

2.3. Fabrication of MEA

Pt/OMC, H_2O and a 5 wt. % of Nafion solution (SIGMA-Aldrich, Co.) with different weight ratios of Pt/OMC versus ionomer solution

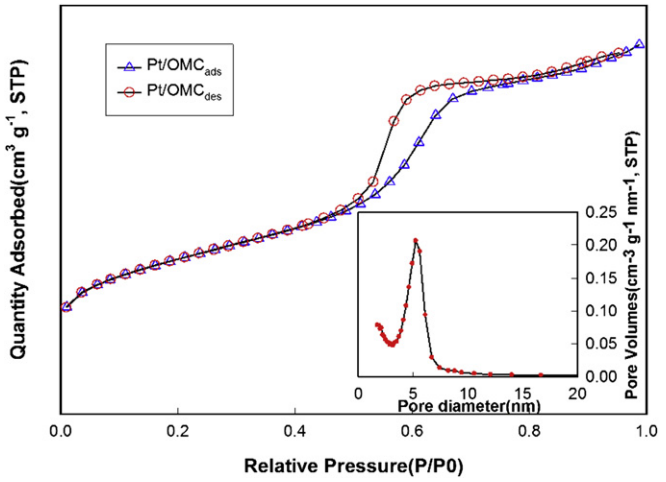

Fig. 2. Isotherm graph of nitrogen adsorption/desorption and pore size distribution (insert) of Pt/OMC.

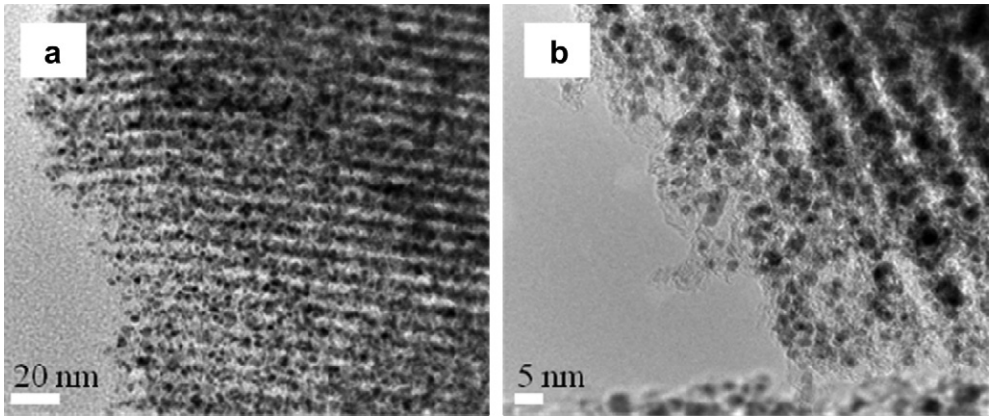

Fig. 3. TEM images of Pt/OMC.

were mixed to prepare the catalyst slurry for the cathode side of the electrode. The weight percent of the ionomer was controlled to be 5, 10, 15, 20 and 30 wt. % of the electrode. After sonication of slurries for 30 min, they were stirred for 30 min at 500 rpm. The anode electrode was fabricated in a manner similar to that of the cathode electrode using commercial Pt/C (40 wt. % Pt/C, HiSPEC™ 4000, Johnson Matthey) and 27.5 wt.% ionomer. Each slurry was placed on the decal substrate, and was then coated at a speed of 3 mm s^{-1}; the temperature was maintained at 303 K during the coating process for effective drying. After drying, decals for the anode and cathode were placed on each side of the membrane (NRE-212, DuPont Inc.) and were then pressed with a pressure of 5 MPa at 130 °C for 4 min. After hot-pressing, substrates were peeled off. MEA with 5, 10, 15, 20 and 30 wt. % of Nafion are denoted by MEA-5, MEA-10, MEA-15, MEA-20 and MEA-30, respectively. The active area of the electrodes was 5 cm^2.

2.4. Physical characteristics of Pt/OMC

The Pt weight percentage of the synthesized Pt/OMC catalyst was measured with a TGA (TA Ins., Q50). BET (Micromertics Ins., ASAP2020) analysis was carried out to measure the specific surface area of the synthesized Pt/OMC catalyst. The shape and dispersion of Pt particles supported on the OMC was examined by TEM (JEM-2010, JEOL). Crystal structure, lattice constant, and mean particle size of the Pt nanoparticles was determined by XRD (Rigaku, RAD-3C) with Cu Kα radiation ($\lambda = 1.541$ Å) and a scan rate of 1.5° min^{-1} from 20 to 100°.

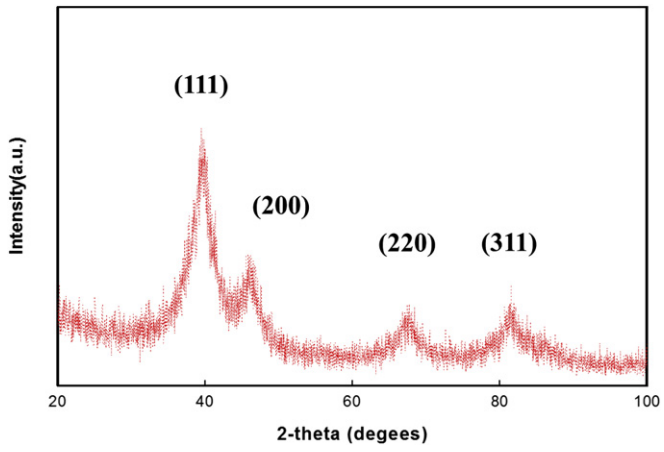

Fig. 4. XRD pattern of prepared Pt/OMCs.

2.5. Electrochemical characterization of single cells

The gas diffusion layers (GDL) (SGL Carbon Inc., Sigracet 10BB) and silicon fabric gaskets (Taconic Co., Ltd.) were used on both sides of the MEAs, and were assembled with a single cell (Fuel Cell Technologies Co.). Hydrogen and air with 100% relative humidity were used as reactants to evaluate the performance of fuel cells at ambient pressure in stoichiometric ratios of 1.5 and 2.0, respectively. The temperature of the single cells was maintained at 343 K. Electrochemical impedance spectroscopy (EIS, Biologic, VMP3B-20 and PC14) was carried out to measure the resistance of the MEA in a frequency range of 0.1 Hz to 10 kHz with a current density of 200 and 800 mA cm^{-2}. Cyclic voltammetry (CV, WonAtech, Gwpg100hp) measurements were performed to identify the electrochemically active surface area at a scan rate of 50 mV s^{-1} supplying 20 sccm of hydrogen and 100 sccm of nitrogen to the anode and cathode, respectively. Pt utilization was calculated by dividing the peak power density by the loading of the prepared cathode catalyst.

3. Results and discussion

3.1. Characterizations of Pt/OMC catalysts

Fig. 1 shows the TGA results. Pt loading in the catalyst was 50.3 wt. %, indicating that Pt particles are well supported on OMCs, as hypothesized. N_2 adsorption and desorption experiments were conducted in order to investigate the pore structure of Pt/OMCs. The isotherm plot (Fig. 2) shows hysteresis when nitrogen absorbs and desorbs on the surface of the catalyst, and the shape of hysteresis is similar to OMC, as reported earlier [18]. Therefore, the major pore structure of the OMCs is not deformed after Pt impregnation. In addition, the BET surface area of the synthesized 50.3 wt. % Pt/OMCs was 616.8 m^2 g^{-1}. According to BET surface area, about half of the pores in OMCs were blocked by dispersed platinum or were lost during Pt/OMC preparation. The total volume of the synthesized catalyst was 0.64 cm^3 g^{-1} and most of that volume (~86%) consisted of mesopores. In addition, BJH adsorption results (Fig. 2 inset) show that the pore size distribution of Pt/OMCs is concentrated around 5 nm, and the average pore diameter of BJH is 4.6 nm. Fig. 3 provides TEM images of Pt/OMC synthesized by the incipient wetness method. OMCs maintain their own structure after Pt impregnation, as observed by BET, and Pt particles are homogeneously dispersed on the support. The average Pt particle size detected by TEM was 2.52 nm. Some Pt particles were between individual ordered carbon nanorods. Fig. 4 shows an XRD pattern of the synthesized catalyst, in which (111), (200), (220), and (311)

Table 1
Summary of characterizations of synthesized Pt/OMCs.

	Pt loading (wt. %)	S_{BET} ($m^2\,g^{-1}$)	V_{total} ($cm^3\,g^{-1}$)	V_{micro} ($cm^3\,g^{-1}$)	V_{meso} ($cm^3\,g^{-1}$)	d_{BJH} (nm)	Pt particle size (nm) by TEM	Pt particle size (nm) by XRD
Pt/OMC	50.3	616.8	0.64	0.09	0.55	4.6	2.52	2.95

peaks clearly demonstrate the face-centered cubic structure of Pt. Using diffraction peaks and the Scherrer equation [39], the mean particle size of Pt on OMCs was calculated to be approximately 2.95 nm. All of the characteristics of the prepared Pt/OMCs are listed in Table 1.

3.2. Electrochemical analysis

The performances of Pt/OMCs with different ionomer contents are shown in Fig. 5. MEA-5 shows a large ohmic loss, which is presumably due to insufficient ionomer content, and allows for transfer of the protons in the electrode, causing a decrease in performance. MEA-20 has the highest potential at the low current density region among the prepared MEAs, indicating that as more ionomer is added to the electrode, the better the performance in the low current density region. However, too much ionomer in the electrode as seen in MEA-30 results in worse performance than MEA-20 due to a trade-off phenomenon in the electrode [36]. In the high current density region, 800 mA cm^{-2}, the order of performances is 10 > 15 > 20 > 5 > 30, and is totally different from the results in the low current density region. At high current density, MEA-5 shows a linear characteristic and MEA-10 shows the highest potential and power density. However, the performances of MEAs decrease as ionomer content increases and MEA-30 therefore presents a lower potential than MEA-5. Over 800 mA cm^{-2}, MEA-20 also shows a significant performance decrease more severe than that of MEA-5. As a result of the polarization curve, MEAs with high ionomer content show better performance at low current density due to their capacity to form a three-phase boundary, but concentration overpotentials are severely increased at high current densities due to interactions between H_2O and Nafion ionomer,

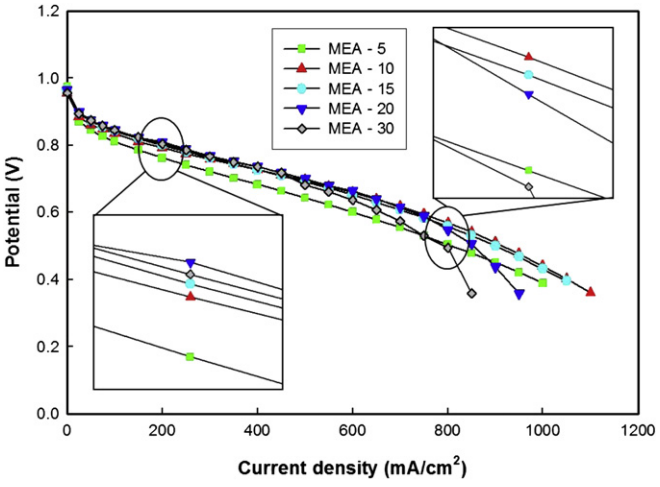

Fig. 5. Polarization curve of MEAs with different ionomer content.

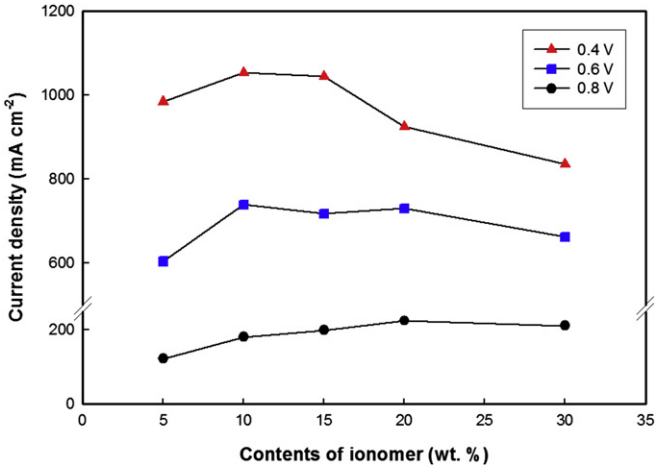

Fig. 6. Current density comparison of MEAs at 0.4, 0.6 and 0.8 V.

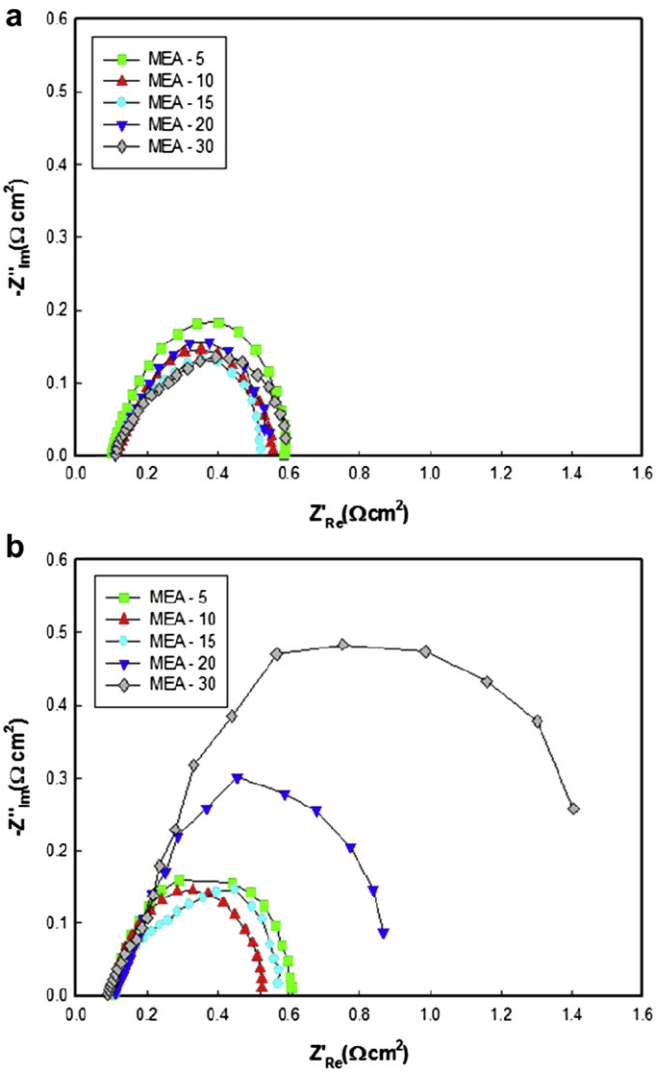

Fig. 7. EIS results of MEA-5 to MEA-30 in (a) low current density region, (b) and high current density region.

Table 2
Summary of electrochemical results of MEAs with different ionomer content.

MEA	Ionomer (wt.%)	Pt loading (mg cm^{-1})	Polarization curve			EIS		CV	Pt utilization (mW mg$_{pt}^{-1}$)
			Current density (mA cm^{-2})			Polarization resistance (Ω_p)		ECSA (m^2 g^{-1})	
			At 0.8 V	At 0.6 V	At 0.4 V	At 200 mA cm^{-2}	At 800 mA cm^{-2}		
MEA-5	5	0.39	122.4	603.3	983.9	0.5905	0.6080	70.1	1044.0
MEA-10	10	0.38	181.3	738.7	1052.4	0.5560	0.5230	91.8	1210.6
MEA-15	15	0.42	199.0	717.6	1043.8	0.5215	0.5705	71.4	1074.5
MEA-20	20	0.40	224.7	729.4	924.1	0.5320	0.8675	79.3	1105.7
MEA-30	30	0.38	211.5	662.2	835.1	0.5890	1.4045	54.4	1058.7

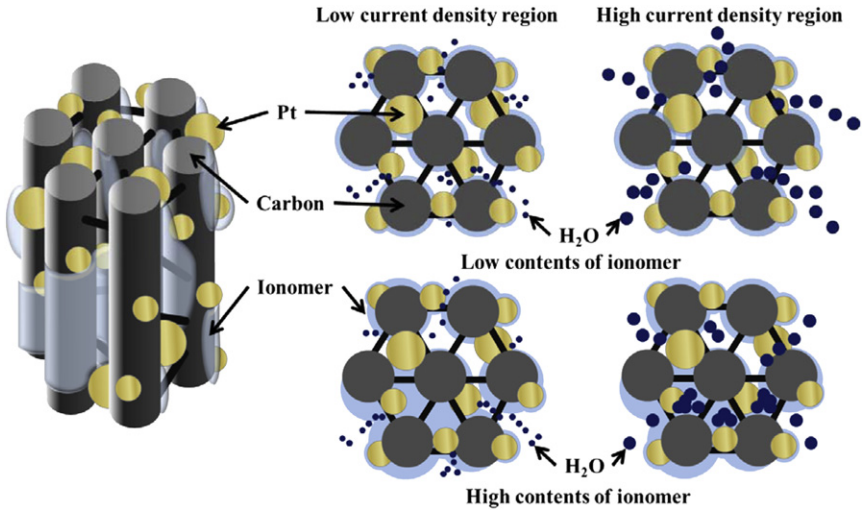

Fig. 8. Schematic illustration for the effect of ionomer contents in the low and high current density regions.

which has hydrophilic characteristics. Fig. 6 is a graph comparing current densities at each potential (0.8, 0.6 and 0.4 V) of MEAs. At 0.8 V, MEA-20 has the highest current density, but MEA-10 shows the best performances at both 0.6 and 0.4 V. Most applications of PEMFCs use a current density around 0.6 V due to its power density and efficiency. Therefore, 10 wt. % of ionomer in the electrode is optimum when synthesized Pt/OMCs is applied for PEMFCs.

The impedance of single cells was analyzed (Fig. 7). At 200 mA cm^{-2}, MEA-5 shows the greatest charge transfer resistance over other MEAs, and MEA-10, 15 and 20 show similar resistances. The charge-transfer resistance of MEA-30 increased as performance decreased. At 800 mA cm^{-2}, the results of EIS were well matched to the performances of the IV curve. Compared with MEA-5, MEA-10 and MEA-15, the charge transfer resistance of MEA-20 and 30 are significantly increased due to high ionomer content. Although MEA-5 showed low potential in the high current density region, it has a smaller charge transfer resistance than MEA-20 because it contains less ionomer, and H_2O produced by electrochemical reactions can easily leave the inside of the electrode and move to the gas diffusion layer.

CV was used to analyze electrochemical active surface area (ECSA), and the results are in Table 2. MEA-10 shows the largest ECSA among MEAs and is compatible with the results of the IV curve and EIS. MEA-5 results in a small ECSA because it cannot provide sufficient proton conduction inside the catalyst layer. However, excessive ionomer in the electrode also resulted in smaller ECSA because it became difficult for reactants such as hydrogen and oxygen to access reactive sites. The best Pt utilizations calculated by both the peak power density and Pt loading were also shown by MEA-10.

Song et al. [40] observed the effects of pore morphology of OMCs, and found that highly ordered structure can yield Pt particles with greater electrochemical surface area, while spaces between nanorods facilitate electrolyte access the to Pt particles. Kim et al. [41] and Liu et al. [42] reported that low ionomer content cannot provide the electrode with mechanical integrity, while a large quantity of ionomers with Pt/OMCs negatively influence performance because spaces between ordered nanorods can be taken up by ionomer, making oxygen diffusion difficult. In addition, the optimum content of ionomer in carbon black based Pt/C is usually between 20 and 40 wt. % of catalyst [26,30,34,35,38]. In this study, however, electrodes with low ionomer content were successfully produced by the decal method, and the unique structure of Pt/OMCs can result in unique conditions in the electrode (Fig. 8). For example, some Pt particles can be placed on two or more hexagonally ordered carbon nanorods (Fig. 3), and can utilize ionomers on each carbon nanorod. Although Pt particles on OMCs can share many electrolytes, too much ionomer may occupy the space in the ordered structure of Pt/OMCs. In the low current density region, this does not matter due to both the small amount of water from the electrochemical reaction and the unique morphology of Pt/OMCs, but it can be a severe problem in the high current density region where a large amount of water may be trapped in the space. Therefore, Pt/OMCs do not require as much ionomer as electrodes with carbon black based Pt/C, and 10 wt. % of ionomer in the electrode is therefore considered an appropriate amount to improve the performance of PEMFCs.

4. Conclusions

Pt/OMCs (50.3 wt. %) were prepared by the incipient wetness method, and Pt particles were well dispersed on the resulting OMCs. The BET surface area was 616.8 m^2 g^{-1} and the average

particle size was 2.52 and 2.95 nm as measured by TEM and XRD, respectively.

MEA-10 shows the best performance at potentials of 0.6 V and 0.4 V, potentials that are commonly used in PEMFC applications. Electrodes with 20 and 30 wt. % ionomer, which is an appropriate content when carbon black is applied as a catalyst support, show large concentration overpotential in the high current density region. EIS results also show a large charge transfer resistance of MEA-20 and MEA-30 at 800 mA cm^{-2}. The highest values of both ECSA and Pt utilization are shown by MEA-10. Pt particles placed on or between two or more carbon nanorods can share and utilize electrolytes, so these Pt/OMCs require less ionomer than catalysts based on carbon black support. However, excessive ionomer can occupy the spaces between ordered structures, and H_2O generated by electrochemical reactions may become trapped in the space, causing mass transfer problems. Therefore, 10 wt. % ionomer with prepared Pt/OMCs is determined to be the optimum amount.

Acknowledgements

This work was supported by 2012 Research Fund of University of Ulsan.

References

[1] R. O'Hayre, S.W. Cha, W. Colella, F.B. Prinz, Fuel Cell Fundamentals, John Wiley & Sons, Hoboken, 2006.
[2] S. Sun, G. Zhang, D. Geng, Y. Chen, R. Li, M. Cai, X. Sun, Angewandte Chemie International Edition 50 (2011) 422–426.
[3] H. Li, G. Sun, N. Li, S. Sun, D. Su, Q. Xin, Journal of Physical Chemistry C 111 (2007) 5605–5617.
[4] D. Lee, S. Hawng, I. Lee, Journal of Power Sources 145 (2005) 147–153.
[5] C.W. Liu, Y.C. Wei, K.W. Wang, Journal of Colloid and Interface Science 325 (2008) 203.
[6] D. Yang, B. Li, H. Zhang, J. Ma, International Journal of Hydrogen Energy 37 (2012) 2447.
[7] D.W. Jung, S. Park, C.Y. Ahn, S.H. Choi, J.B. Kim, Korean Journal of Materials Research 19 (2009) 667.
[8] K.H. Lim, H.S. Oh, H.S. Kim, Electrochemical Communications 11 (2009) 1131.
[9] F. Yuan, H.K. Yu, H. Ryu, Electrochimica Acta 50 (2004) 685.
[10] N. Rajalakshmi, H. Ryu, M.M. Shaijumon, S. Ramaprabhu, Journal of Power Sources 140 (2005) 250.
[11] S. Sharma, B.G. Pollet, Journal of Power Sources 208 (2012) 96.
[12] G. Hoogers, Fuel Cell Technology Handbook, CRC Press, Boca Raton, Fl, 2003.
[13] S.H. Joo, S.J. Choi, I. Oh, J. Kwak, Z. Liu, O. Terasaki, R. Ryoo, Nature 412 (2001) 169.
[14] L.Y. Bian, Y.H. Wang, J.B. Zang, J.K. Yu, H. Huang, Journal of Electroanalytical Chemistry 644 (2010) 85.
[15] S. Liu, J. Wang, J. Zeng, J. Ou, Z. Li, X. Liu, S. Yang, Journal of Power Sources 195 (2010) 4628.
[16] S. Jun, S.H. Joo, R. Ryoo, M. Kruk, M. Jaroniec, Z. Liu, T. Ohsuna, O. Terasaki, Journal of the American Chemical Society 122 (2000) 10712.
[17] C.H. Kim, D.K. Lee, T.J. Pinnavaia, Langmuir 20 (2004) 5157.
[18] S.H. Joo, C. Park, D.J. You, S.A. Lee, H.I. Lee, J.M. Kim, H. Chang, D. Seung, Electrochimica Acta 52 (2006) 1618.
[19] J.B. Joo, P. Kim, W. Kim, J. Yi, Journal of Electoceramics 17 (2006) 713.
[20] S.H. Joo, K. Kwon, D.J. You, C. Park, H. Chang, J.M. Kim, Electrochimica Acta 54 (2009) 5746.
[21] E.P. Ambrosio, C. Francia, M. Manzoli, N. Penazzi, P. Spinelli, International Journal of Hydrogen Energy 33 (2008) 3142.
[22] L. Calvillo, M. Gangeri, S. Perathoner, G. Centi, R. Moliner, M.J. Lázaro, International Journal of Hydrogen Energy 36 (2011) 9805.
[23] Y. Ma, L. Cui, J. He, T. Wang, Y. Guo, J. Tang, C. Li, Y. Hu, H. Xue, M. Liu, X. Sun, Electrochimica Acta 63 (2012) 318.
[24] E. Passalacqua, F. Lufrano, G. Squadrito, A. Patti, L. Giorgi, Electrochimica Acta 46 (2001) 799.
[25] G. Sasikumar, J.W. Ihm, H. Ryu, Electrochimica Acta 132 (2004) 11.
[26] S.H. Choi, D.W. Jung, S.O. Yoon, S. Park, E.S. Oh, J. Kim, Metals and Materials International 17 (2011) 811.
[27] S.J. Lee, S. Mukerjee, J. McBreen, Y.W. Rho, Y.T. Kho, T.H. Lee, Electrochimica Acta 43 (1998) 3693.
[28] M. Zhiani, H. Gharibi, K. Kakaei, International Journal of Hydrogen Energy 35 (2010) 9261.
[29] A.M. Chaparro, B. Gallardo, M.A. Folgado, A.G. Martín, L. Daza, Catalysis Today 143 (2009) 237.
[30] G. Sasikumar, J.W. Ihm, H. Ryu, Electrochimica Acta 50 (2004) 601.
[31] D. Lee, S. Hwang, International Journal of Hydrogen Energy 33 (2008) 2790.
[32] C.M. Lai, J.C. Lin, F.P. Ting, S.D. Chyou, K.L. Hsueh, International Journal of Hydrogen Energy 33 (2008) 4132.
[33] T. Suzuki, S. Tsushima, S. Hirai, International Journal of Hydrogen Energy 36 (2011) 12361.
[34] K.H. Kim, H.J. Kim, K.Y. Lee, J.H. Jang, S.Y. Lee, E. Cho, I.H. Oh, T.H. Lim, International Journal of Hydrogen Energy 33 (2008) 2783.
[35] K.H. Kim, K.Y. Lee, H.J. Kim, E. Cho, S.Y. Lee, T.H. Lim, S.P. Yoon, I.C. Hwang, J.H. Jang, International Journal of Hydrogen Energy 35 (2010) 2119.
[36] J.H. Jung, D.W. Jung, J. Kim, Journal of Korean Electochemical Society 14 (2011) 50.
[37] S. Du, B. Millington, B.G. Pollet, International Journal of Hydrogen Energy 36 (2011) 4386.
[38] S. Jeon, J. Lee, G.M. Rios, H.J. Kim, S.Y. Lee, E. Cho, T.H. Lim, J.H. Jang, International Journal of Hydrogen Energy 35 (2010) 9678.
[39] Z. Liu, L.M. Gan, L. Hong, W. Chen, J.Y. Lee, Journal of Power Sources 139 (2005) 73.
[40] S. Song, Y. Liang, Z. Li, Y. Wang, R. Fu, D. Wu, P. Tsiakaras, Applied Catalysis B: Environment 98 (2010) 132.
[41] H.T. Kim, D.J. You, H.K. Yoon, S.H. Joo, C. Park, H. Chang, I.S. Song, Journal of Power Sources 180 (2008) 724.
[42] B. Liu, S. Creager, Electrochimica Acta 55 (2010) 2721.